Chemical Science

ROYAL SOCIETY OF CHEMISTRY

EDGE ARTICLE

View Article Online
View Journal | View Issue



Cite this: *Chem. Sci.*, 2023, **14**, 5425

All publication charges for this article have been paid for by the Royal Society of Chemistry

Received 4th January 2023
Accepted 25th April 2023

DOI: 10.1039/d3sc00035d

rsc.li/chemical-science



# Regulating supramolecular interactions in dimeric macrocycles†

Pengwei Fang,[ab] Muqing Chen, *[ab] Nan Yin,[b] Guilin Zhuang, *[c] Tianyun Chen,[b] Xinyu Zhang[b] and Pingwu Du *[b]

Supramolecular behavior is highly dependent on many factors, including complicated microenvironments and weak interactions. Herein, we describe tuning supramolecular architectures of rigid macrocycles by synergistic effects of their geometric configurations, sizes, and guests. Two paraphenylene-based macrocycles are anchored onto different positions in a triphenylene derivative, resulting in dimeric macrocycles with different shapes and configurations. Interestingly, these dimeric macrocycles show tunable supramolecular interactions with guests. In solid state, a 2 : 1 host–guest complex was observed between **1a** and $C_{60}$/$C_{70}$, while an unusual 2 : 3 host–guest complex $3C_{60}$@(**1b**)$_2$ can be observed between **1b** and $C_{60}$. This work expands the scope of the synthesis of novel rigid bismacrocycles and provides a new strategy to construct different supramolecular systems.

## Introduction

Fullerene is one of the most extensively studied carbon nanomaterials in recent decades due to its unique chemical and electrical properties.[1–3] In particular, the encapsulation of fullerenes by some specific host molecules *via* π–π interaction has attracted much attention because of their potential applications in the separation, solubilization, and chemical modification of fullerenes.[4–6] Generally, an ideal host molecule should satisfy both the structural and electronic complementarity with spherical fullerenes.[7] Thus electron-rich macrocyclic structures, such as azacrown ethers,[8] calixarenes,[9] tetrathiafulvalenes-based macrocycles,[10] pillararenes,[11] and porphyrinylene nanohoops,[12] have long been considered as promising hosts in fullerene-containing host–guest systems. Their shape complementarity greatly improves the recognition abilities and selectivities toward fullerenes.[10,13] Over the past decade, carbon-rich cycloparaphenylene macrocycles and their derivatives were reported as interesting host molecules in the study of π–π interactions with $C_{60}$ or other fullerenes.[14–18] These macrocycles usually exhibit good π–π interactions with fullerenes or their derivatives in a 1 : 1 ratio. It would be intriguing if one could manipulate the supramolecular characteristics of these macrocycles to construct novel supramolecular donor–acceptor–donor (D–A–D) systems,[19] for example, two macrocycles cooperate to bind a fullerene molecule rather than the typical one-to-one complexing (Fig. 1a).

The hosting of fullerene molecules in the cavity is mainly influenced by the ring size, geometric configuration, microenvironment, functional groups, fullerene size, and even solvent (Fig. 1b). To date, previous studies showed that only modifying a single macrocycle cannot fully achieve the abovementioned

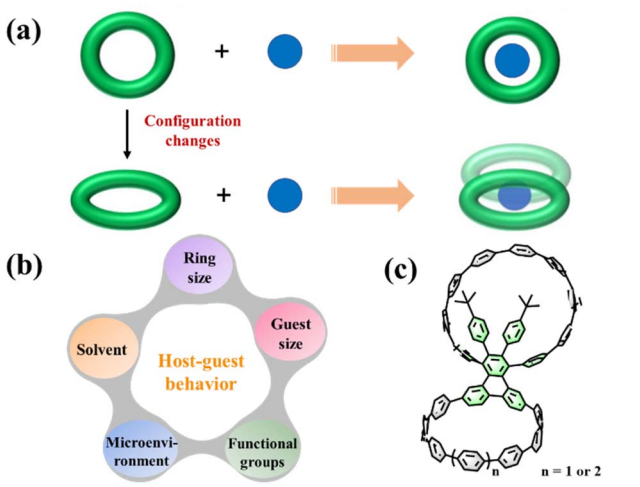


Fig. 1 (a) Tuning supramolecular characteristics of conjugated macrocycles to construct an unconventional host–guest system. (b) Several factors affecting host–guest behaviors. (c) Molecular structures of bismacrocycles **1a** and **1b**.

[a]*School of Environment and Civil Engineering, Dongguan University of Technology, Dongguan, 523808, Guangdong Province, China. E-mail: mqchen@ustc.edu.cn*

[b]*Key Laboratory of Precision and Intelligent Chemistry, Hefei National Research Center for Physical Sciences at the Microscale, Anhui Laboratory of Advanced Photon Science and Technology, Department of Materials Science and Engineering, University of Science and Technology of China, 96 Jinzhai Road, Hefei, 230026, Anhui Province, China. E-mail: dupingwu@ustc.edu.cn*

[c]*College of Chemical Engineering, Zhejiang University of Technology, 18 Chaowang Road, Hangzhou, 310032, Zhejiang Province, China. E-mail: glzhuang@zjut.edu.cn*

† Electronic supplementary information (ESI) available. CCDC 2191567, 2191568 and 2161639. For ESI and crystallographic data in CIF or other electronic format see DOI: https://doi.org/10.1039/d3sc00035d

goals.[20–22] Recently, the development of cycloparaphenylene bismacrocycles enriches the family of fullerene-containing supramolecular systems with a high stoichiometry ratio and tunable cavity shapes.[23–26] For example, Cong and coworkers employed a cyclooctatetrathiophene unit as the linker to build a figure-of-eight bismacrocycle whose adaptive cavities enable the formation of peanut-like 1 : 2 host–guest complexes with $C_{60}$ or $C_{70}$.[25] Notably, these bismacrocycles often have two macrocycles with the same sizes, shapes, and supramolecular properties because there are no other aryl groups at the linker that can affect the microenvironment of the bismacrocycle. Based on this, we envision that the geometric configurations could be finely tuned when these macrocycles are formed with different microenvironments, resulting in different and interesting supramolecular properties.

Herein, we report the design and synthesis of two novel dimeric macrocycles **1a** and **1b**, in which two cycloparaphenylene macrocycles with tunable sizes are anchored onto a triphenylene derivative (Fig. 1c). Interestingly, **1a** exhibits a very weak host ability and can only capture one $C_{60}$ or $C_{70}$ molecule to form 2 : 1 host–guest complexes by cooperating with another bismacrocycle. By changing the ring size, another bismacrocycle **1b** can interact with three $C_{60}$ molecules to construct a 2 : 3 host–guest complex, demonstrating the first 2 : 3 host–guest complex in the supramolecular chemistry of bismacrocycles.

## Results and discussion

### Molecular design and synthesis

To compare the effect of microenvironments on a host–guest system, it is important to rationally select the appropriate building blocks and synthesis strategy to construct a bismacrocycle with different geometric configurations. In this work, a triphenylene derivative, 1,4-bis(4-bromophenyl)-2,3-bis(4-*tert*-butylphenyl)-6,11-diiodotriphenylene, is used; it is a suitable precursor since these halogen groups can provide different reactive sites for subsequent macrocycle formations, whereas the peripheral 4-*tert*-butylphenyl groups can influence the geometrical environment of the macrocycle to which it is connected. A prior study showed that a cyclic fragment can selectively react with the iodine groups within this precursor to form a bifunctional macrocyclic structure.[27] Inspired by this report, we can choose different curved synthones to react with this triphenylene derivative *via* the Suzuki coupling reaction and aromatization reaction to give target bismacrocycles with different sizes.

The rate of oxidative addition in a Suzuki–Miyaura reaction is largely controlled by the bond dissociation energies (BDEs) of C–X (X = I, Br, Cl) bonds.[28,29] The key point in this strategy is to take advantage of the difference in BDEs between Ar–I and Ar–Br bonds (Ar–I > Ar–Br) to allow for a selective reaction in the ring formations. The synthetic strategy for **1a** and **1b** is shown in Fig. 2. Starting materials **2a**, **2b**, and **3** were prepared according to the reported literature.[27,30,31] Initially, diboronate **2a** was selectively reacted with the iodine groups in compound **3** to prepare bifunctional macrocycle **4a** under relatively weak

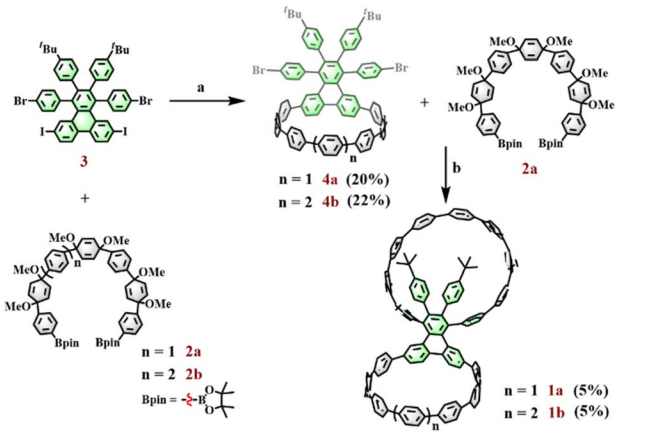


Fig. 2 Reaction conditions: (a) (1) $Pd(PPh_3)_4$, $K_2CO_3$, THF, $H_2O$, 68 °C; (2) $H_2SnCl_4$, THF, rt. (b) (1) $Pd_2(dba)_3$, S-Phos, $Cs_2CO_3$, toluene, MeOH, $H_2O$, 100 °C; (2) $H_2SnCl_4$, THF, rt.

reaction conditions (catalyst: $Pd(PPh_3)_4$; base: $K_2CO_3$) and subsequent reductive aromatization with $H_2SnCl_4$. With this key fragment **4a** in hand, the second intermolecular cyclization between **4a** and **2a** was performed under strong Suzuki coupling reaction conditions (catalyst: $Pd_2(dba)_3$, S-Phos; base: $Cs_2CO_3$) and subsequent reductive aromatization with $H_2SnCl_4$ to afford the target bismacrocycle **1a**. It is worth noting that the two-step macrocyclization strategy can significantly improve the yield of the target bismacrocycle when compared to the one-pot method. By applying this strategy, another bismacrocycle **1b** could also be prepared by replacing compound **2a** with its 8-ring partner **2b**. Following a similar procedure to that of **1a**, diboronate **2b** coupled with **3** to give key macrocycle **4b**, which then underwent the second Suzuki macrocyclization with **2a** and subsequent reductive aromatization to deliver bismacrocycle **1b**.

### Physical characterizations

The successful synthesis of **1a** and **1b** was confirmed by a combination of MALDI-TOF mass spectrometry, nuclear magnetic resonance (NMR), and X-ray crystallography. The peaks found at *m*/*z* 1705.7546 and 1781.7811 (calculated for **1a**: $C_{134}H_{96}$ $[M]^+$ 1705.7501; **1b**: $C_{140}H_{100}$ $[M]^+$ 1781.7859) suggested successful synthesis of the target compounds. Further characterization by $^1$H NMR spectroscopies also confirmed the successful synthesis of **1a** and **1b**. As shown in Fig. 3a, the characteristic singlet at $\delta$ = 8.34 ppm can be assigned to $\mathbf{H_1}$ because its vicinal positions are all quaternary carbons. The multiplets at $\delta$ = 7.43–7.63 ppm ($\mathbf{H_7}$) are mainly from the protons in the cycloparaphenylene moieties according to the overlapped peak shape, chemical shifts and number of integral protons. To fully assign all the protons in **1a**, we recorded the 2D $^1$H–$^1$H COSY NMR spectrum (Fig. 3b). The doublet at $\delta$ = 7.78 ppm is correlated with the signals at $\delta$ = 8.34 ppm and 8.30 ppm, suggesting that the doublets at $\delta$ = 7.78 ppm and 8.30 ppm can be assigned to $\mathbf{H_2}$ and $\mathbf{H_3}$, respectively. Three doublets at $\delta$ = 7.20 ppm, 7.34 ppm, and 7.39 ppm are strongly

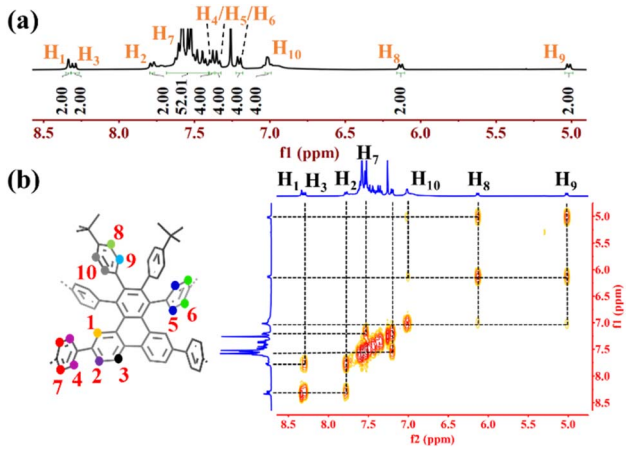


Fig. 3 (a) Aromatic regions of the $^{1}$H NMR spectrum of **1a**. (b) Expanded 2D $^{1}$H–$^{1}$H COSY NMR spectrum of **1a**.

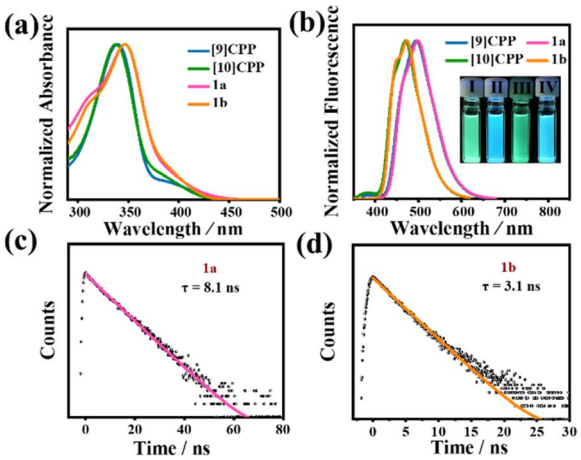


Fig. 4 (a) UV-vis absorption of $CH_2Cl_2$ solutions of **1a**, **1b**, [9]CPP and [10]CPP. (b) Fluorescence spectra of the $CH_2Cl_2$ solutions of **1a**, **1b**, [9]CPP and [10]CPP. Inset: photographs showing the fluorescence for **1a** (I), **1b** (II), [9]CPP(III), and [10]CPP(IV) in $CH_2Cl_2$ under a UV lamp at $\lambda$ = 365 nm. (c) Emission lifetime for **1a**. (d) Emission lifetime for **1b**.

correlated with the signals at $\delta$ = 7.43–7.63 ppm, confirming that those signals belong to $\mathbf{H_4}$, $\mathbf{H_5}$, and $\mathbf{H_6}$. Another three signals at $\delta$ = 5.02 ppm, 6.13 ppm, and 7.00 ppm show no interactions with the protons of cycloparaphenylene moieties, implying that they may originate from phenyl groups connected to the *tert*-butyl groups. Combined with the crystal data, protons $\mathbf{H_8}$ and $\mathbf{H_9}$ could be located in the shielding region induced by the macrocyclic ring current, forcing their chemical shifts to the high field. Therefore, the doublets at $\delta$ = 5.02 ppm and 6.13 ppm can be ascribed to $\mathbf{H_8}$ and $\mathbf{H_9}$, respectively, and the signal at $\delta$ = 7.00 ppm can be assigned to $\mathbf{H_{10}}$. Similar assignments can be made for the protons in **1b**.

## Photophysical properties

The photophysical properties of **1a** and **1b** were studied by UV-vis absorption spectroscopy, steady-state fluorescence spectroscopy, and time-resolved fluorescence decay. Interestingly, the absorption and fluorescence spectra of **1a** and **1b** both reveal unique features of this type of bismacrocycle compared with [9]CPP and [10]CPP (Fig. 4a and b). No significant difference is found in the absorption spectra of **1a** and **1b**; their maximum absorption peaks are located at 346.5 nm and 346 nm, respectively (molecular absorption coefficients $\varepsilon_{\mathbf{1a}}$ = $1.54 \times 10^4$ M$^{-1}$ cm$^{-1}$, $\varepsilon_{\mathbf{1b}} = 9.01 \times 10^4$ M$^{-1}$ cm$^{-1}$), which are slightly redshifted compared to [*n*]CPPs.[32] To identify the difference in optical properties, time-dependent density functional theory (TD-DFT) with PBE0/6-31G(d,p)//PCM was performed. The calculation results reveal that the observed experimental peak at 346.5 nm in **1a** mainly corresponds to the HOMO−2 → LUMO and HOMO → LUMO+2 electronic transitions, while the peak at 346 nm in **1b** corresponds to the HOMO → LUMO+1 and HOMO−4 → LUMO transitions. In the fluorescence spectra, **1a** is nearly identical to that of [9]CPP with no traces of the fluorescence peaks that originated from [10]CPP. Similarly, **1b** also only exhibits the fluorescence features of [10]CPP, whereas the addition of another macrocycle has no effect on its fluorescence properties. The fluorescence quantum yields ($\Phi_F$) of **1a** and **1b** were estimated to be approximately 12.9% and 7.5%, respectively. Under irradiation by a hand-held UV lamp at $\lambda$ = 365 nm, the photoluminescence of the diluted solution ($1.0 \times 10^{-5}$ M) of **1a** and **1b**, *i.e.*, green and cyan, respectively, are also the same as those of [9]CPP and [10]CPP, which are consistent with the results of the fluorescence spectroscopy. The luminescence lifetimes ($\tau_s$) of **1a** and **1b** were measured by time-resolved fluorescence decay using the time-resolved photoluminescence (TRPL) technique (Fig. 4c and d). When excited at 390 nm, the $\tau_s$ of **1a** and **1b** were determined to be approximately 8.1 ns at 499 nm and 3.1 ns at 475 nm, respectively, using single-exponential decay fitting.

## Supramolecular chemistry in the solid-state and solution

Analogous to the fullerene hosting properties of [10]CPP,[17,33,34] slow liquid diffusion of hexane into a chlorobenzene solution containing **1a** and excess $C_{60}$ or $C_{70}$ afforded black single crystals suitable for single-crystal X-ray measurements. The crystal structure not only unambiguously validates the composition and stereochemistry of **1a** but also reveals intriguing and unexpected host–guest properties. Notably, two **1a** molecules are bridged by a $C_{60}$ or $C_{70}$ molecule to build the 2 : 1 host–guest systems, in which the $C_{60}$ or $C_{70}$ molecule is shared by two [10]CPP moieties from different **1a** molecules. As shown in the crystal structure of $C_{60}$@(**1a**)$_2$ (Fig. 5a), the host moiety exhibits an oval shape with long and short axes of 14.12 Å and 13.15 Å, respectively. The interfacial distances between the host moieties and $C_{60}$, defined as the distance between the centroid of a benzene unit of the macrocycle and the nearest centroid of a hexagon or pentagon of $C_{60}$, are mostly greater than 4.0 Å with only a few parts less than 3.8 Å (highlighted in red, more detailed information see in Fig. S12†), implying that only a few aromatic rings participate in the convex–concave π–π stacking interactions and that the supramolecular interactions are quite weak. Therefore, a single oval-shaped macrocycle cannot capture a $C_{60}$ molecule but rather can only bind that molecule

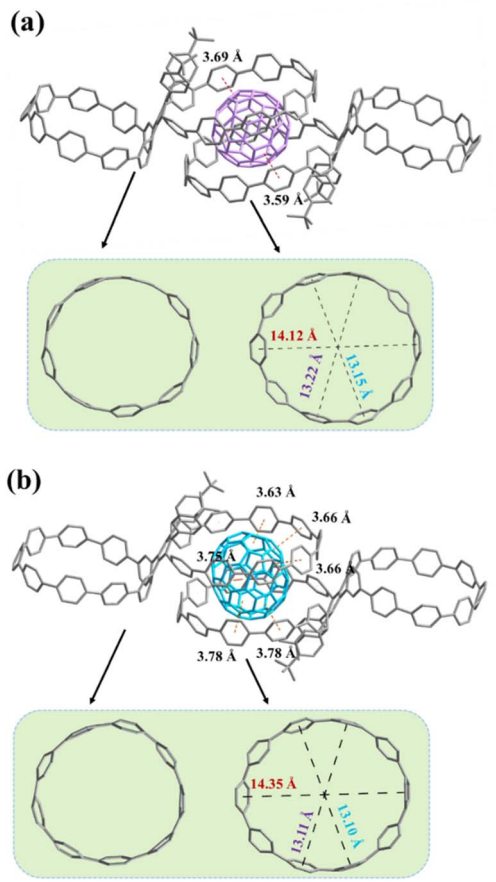


Fig. 5 (a) Crystal structure of $C_{60}$@(**1a**)$_2$. (b) Crystal structure of $C_{70}$@(**1a**)$_2$. Hydrogen atoms and disordered solvent molecules are omitted for clarity.

by cooperating with the same oval-shaped macrocycle from another bismacrocycle. This behavior is probably because the oval-shaped macrocycle configuration and the steric hindrance of *tert*-butylphenyl groups change the supramolecular interactions between the conjugated macrocycle and $C_{60}$. Due to the unique ellipsoid shape, the interfacial distances between $C_{70}$ and the host moieties are relatively smaller than those of $C_{60}$ but also show the weak supramolecular interactions (Fig. 5b, the distances less than 3.8 Å are highlighted in orange and more detailed information see in Fig. S15†). Interestingly, $C_{60}$@(**1a**)$_2$ is aligned in a linear manner, while $C_{70}$@(**1a**)$_2$ exhibits a herringbone alignment style (Fig. S14 and S17†). It should be mentioned that there are no significant intermolecular interactions between $C_{60}$@(**1a**)$_2$ and $C_{70}$@(**1a**)$_2$ molecules.

Encouraged by these results, we are able to build the first 2 : 3 host–guest system between **1b** and $C_{60}$. By slow evaporation of toluene solutions containing **1b** and excess $C_{60}$, black single crystals suitable for X-ray measurements can be obtained. As shown in Fig. 6, the two macrocycles within **1b** show different geometric shapes: one is approximately circular with an inner diameter of (13.66 ± 0.28) Å, and the other is oval with long and short axes of 14.38 Å and 12.8 Å, respectively. The crystal structure reveals that two **1b** molecules interact with three $C_{60}$ molecules to form a five-membered complex, with each circular

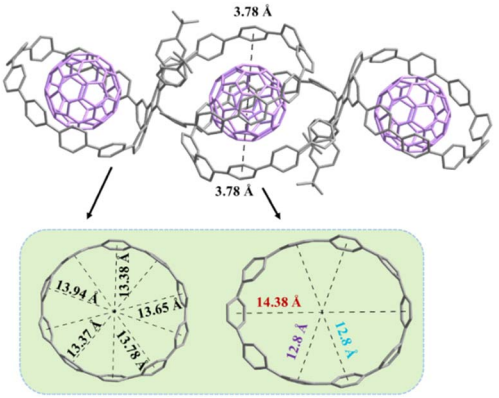


Fig. 6 Crystal structure of 3$C_{60}$@(**1b**)$_2$. Hydrogen atoms and disordered solvent molecules are omitted for clarity.

macrocycle binding one $C_{60}$ molecule and two oval-shaped macrocycles just sharing one. The interfacial distances between $C_{60}$ and the circular macrocycle are found to be within the range of 3.58–3.91 Å (only three are more than 3.80 Å), demonstrating strong π–π stacking interactions. However, the interfacial distances between $C_{60}$ and the oval-shaped macrocycle are mostly greater than 4.0 Å, indicating a weak π–π stacking interaction (the distances less than 3.8 Å are highlighted in black and more detailed information see in Fig. S18†). Similarly, 3$C_{60}$@(**1b**)$_2$ molecules align in a herringbone manner, and no significant intermolecular interactions have been observed between 3$C_{60}$@(**1b**)$_2$ molecules (Fig. S20†).

Although crystallographic data can accurately characterize a host–guest complex, the crystalline structure does not mean it will adopt the same conformation in solution or other phases.[35] Supramolecular chemistry in dilute solution differs from the supramolecular assembly behavior of **1a** and **1b** with $C_{60}$ or $C_{70}$ in the solid-state in that weak interactions are influenced by both the molecular structure and the solvent. According to the MALDI-TOF mass spectrum and fluorescence quenching measurements, no supramolecular interaction was observed between **1a** and $C_{60}$ or $C_{70}$ in solution. The reason for this phenomenon may be that the very weak supramolecular interaction between [10]CPP moieties within **1a** and fullerenes dissociated by the solvent molecule. However, the interaction between **1b** and $C_{60}$ can be clearly observed when $C_{60}$ was added to a solution of **1b**, resulting in a distinct color change from cyan to brown and a reduced fluorescence intensity. The MALDI-TOF mass spectrum displayed a peak at *m*/*z* 2502.7812 (calculated for $C_{200}H_{100}$ [$C_{60}$@**1b**]$^+$: 2502.7892), indicating the formation of a 1 : 1 complex (Fig. S21†). This apparent contradictory host–guest ratio has also been observed in other fullerene-based supramolecular complexes.[36,37] Since there is only a size difference between these two bismacrocycles, we speculate that the supramolecular interaction mainly occurs between the circular macrocycle within **1b** and $C_{60}$, so that only 1 : 1 complex can be detected by mass spectrum. In order to quantitatively investigate the supramolecular assembly of **1b** with $C_{60}$, we carried out fluorescence measurements with an excitation wavelength of 320 nm. Upon gradual addition of $C_{60}$

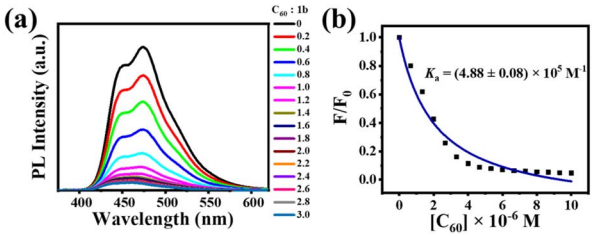


Fig. 7 (a) Fluorescence spectra of **1b** ($3.33 \times 10^{-6}$ M) in the presence of $C_{60}$ in toluene. The concentrations of $C_{60}$ ranged from 0 to $1.0 \times 10^{-5}$ M. (b) Plot of the absorption changes at 474 nm *versus* [$C_{60}$] in toluene for calculating the binding constant.

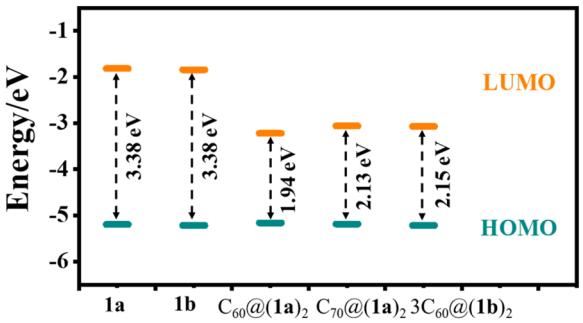


Fig. 8 Schematic diagram illustrating the frontier orbital energy levels of **1a**, **1b**, $C_{60}$@(**1a**)$_2$, $C_{70}$@(**1a**)$_2$, and $3C_{60}$@(**1b**)$_2$.

to the solution of **1b**, the fluorescence intensity of **1b** dramatically decreased, as shown in Fig. 7a. Based on the quenching results, the binding constant was calculated to be approximately $K_a = (4.88 \pm 0.08) \times 10^5$ M$^{-1}$ (Fig. 7b). The deviation between the fitted isotherm and the experimental data could be attributed to the very weak interaction between the oval-shaped macrocycle and $C_{60}$ in solution. Furthermore, experimental data points were fitted to a standard 1 : 1 stoichiometry and different types of 1 : 2 stoichiometries according to the reported methods,[38–40] but all the fitting errors were large (the minimum error is greater than 13%, more detailed information see in Fig. S22–S26†), indicating that the supramolecular interaction between **1b** and $C_{60}$ is difficult to achieve perfect equilibrium of 1 : 1 or 1 : 2 in solution. Recently, it has been reported that a chrysenylene-based carbon macrocycle can interact with $C_{70}$ in 1 : 1, 1 : 2, and 2 : 1 stoichiometries in solution, which is significantly different from crystal structures.[41] Even for a simple CPP macrocycle, von Delius and coworkers demonstrated complicated supramolecular interactions between [10]CPP and fullerenes, where 1 : 1 and 2 : 1 complexes of [10]CPP and $C_{60}$/$C_{70}$ were detected in solution.[42] Therefore, after many attempts, we still failed to obtain the accurate supramolecular complexation stoichiometry of **1b** and $C_{60}$ in solution, indicating a similar complicated complexation in solution and a huge challenging determination of stoichiometry. Fortunately, we have successfully obtained the crystal structures of the complexes of these two bismacrocycles and fullerenes, which allowed us to precisely determine the stoichiometries of these complexes in the solid state.

### Theoretical calculations

Geometrical optimization was carried out at the theoretical level of B3LYP/6-31G(d,p), where DFT-D3(BJ) and polarizable continuum model (PCM) methodologies can be used to correct the dispersion energy and solvent effect of dichloromethane.[43,44] The calculation results show that two *tert*-butylbenzene groups lie at an average angle of 73.28° for **1a** and 74.79° for **1b** with a bridging phenyl in the [10]CPP moiety. Unexpectedly, the strain energies of **1a** and **1b** are as high as 103.12 kcal mol$^{-1}$ and 103.19 kcal mol$^{-1}$, respectively. Compared with [9]CPP (64.71 kcal mol$^{-1}$) and [10]CPP (59.47 kcal mol$^{-1}$), the strain energies of **1a** and **1b** increase dramatically, which can be attributed to the unique topological structure. The frontier molecular orbitals of **1a**, **1b**, $C_{60}$@(**1a**)$_2$, $C_{70}$@(**1a**)$_2$, and $3C_{60}$@(**1b**)$_2$ are shown in Fig. S28–S32.† Due to the structural similarity, **1a** and **1b** possess almost the same occupied molecular orbitals and unoccupied molecular orbitals and thus have similar HOMO–LUMO gaps (~3.38 eV). However, their inclusion complexes of $C_{60}$ or $C_{70}$ feature a downshift of the unoccupied molecular orbital and an upshift of the occupied molecular orbitals, and the HOMO–LUMO gaps decreases (Fig. 8).

## Conclusions

In summary, we have designed and synthesized two dimeric macrocycles by anchoring two cycloparaphenylene macrocycles on a triphenylene derivative. These two bismacrocycles show interesting photophysical properties: the absorption spectra of **1a** and **1b** are almost identical, whereas the fluorescence spectra of **1a** and **1b** are quite different. The unique structure of the triphenylene derivative allows two macrocycles to be under different microenvironments, which in turn generate varying geometric configurations and supramolecular properties. Notably, the macrocycles within the bismacrocycles show supramolecular behaviors distinct from those of pristine units. In the solid-state, two **1a** molecules cooperate to bind a $C_{60}$ or $C_{70}$ molecule to build the 2 : 1 host–guest complexes, while two **1b** molecules and three $C_{60}$ molecules can form a 2 : 3 host–guest complex. Interestingly, **1b** can binds one $C_{60}$ molecule in a 1 : 1 ratio to build another host–guest system in solution due to the weak host ability of the oval-shaped macrocycle. All these results show that the supramolecular properties of dimeric macrocycles can be finely tuned by their configurations, microenvironments, and even solvents.

## Data availability

Experimental procedures, characterization data, titration experiments, and computational data are available in the ESI.†

## Author contributions

P. D. conceived and designed this research with the help of M. C. and P. F. The manuscript was written through contributions

of all authors. All authors have given approval to the final version of the manuscript.

## Conflicts of interest

There are no conflicts to declare.

## Acknowledgements

This work was financially supported by the National Natural Science Foundation of China (22225108, 21971229, U1932214, 52172053).

## Notes and references

1 I. Hiroshi, H. Kiyoshi, A. Tsuyoshi, A. Masanori, T. Seiji, O. Tadashi, S. Masahiro and S. Yoshiteru, *Chem. Phys. Lett.*, 1996, **263**, 545–550.
2 H. W. Kroto, J. R. Heath, S. C. O'Brien, R. F. Curl and R. E. Smalley, *Nature*, 1985, **318**, 162–163.
3 M. Prato, *J. Mater. Chem.*, 1997, **7**, 1097–1109.
4 D. Canevet, E. M. Pérez and N. Martín, *Angew. Chem., Int. Ed.*, 2011, **50**, 9248–9259.
5 F. Diederich and M. Gómez-López, *Chem. Soc. Rev.*, 1999, **28**, 263–277.
6 E. M. Pérez and N. Martín, *Chem. Soc. Rev.*, 2008, **37**, 1512–1519.
7 C. García-Simón, M. Costas and X. Ribas, *Chem. Soc. Rev.*, 2016, **45**, 40–62.
8 J. Effing, U. Jonas, L. Jullien, T. Plesnivy, H. Ringsdorf, F. Diederich, C. Thilgen and D. Weinstein, *Angew. Chem., Int. Ed. Engl.*, 1992, **31**, 1599–1602.
9 J. L. Atwood, G. A. Koutsantonis and C. L. Raston, *Nature*, 1994, **368**, 229–231.
10 J. Calbo, A. de Juan, J. Aragó, J. Villalva, N. Martín, E. M. Pérez and E. Ortí, *Phys. Chem. Chem. Phys.*, 2019, **21**, 11670–11675.
11 H. Li, Q. Chen, C. Schönbeck and B.-H. Han, *RSC Adv.*, 2015, **5**, 19041–19047.
12 Y. Xu, S. Gsänger, M. B. Minameyer, I. Imaz, D. Maspoch, O. Shyshov, F. Schwer, X. Ribas, T. Drewello, B. Meyer and M. von Delius, *J. Am. Chem. Soc.*, 2019, **141**, 18500–18507.
13 Q. Shi, X. Wang, B. Liu, P. Qiao, J. Li and L. Wang, *Chem. Commun.*, 2021, **57**, 12379–12405.
14 W. Li, F. Qu, L. Liu, Z. Zhang, J. Liang, Y. Lu, J. Zhang, L. Wang, C. Wang and T. Wang, *Angew. Chem., Int. Ed.*, 2022, **61**, e202116854.
15 D. Lu, G. Zhuang, H. Wu, S. Wang, S. Yang and P. Du, *Angew. Chem., Int. Ed.*, 2017, **56**, 158–162.
16 S. Wang, X. Li, X. Zhang, P. Huang, P. Fang, J. Wang, S. Yang, K. Wu and P. Du, *Chem. Sci.*, 2021, **12**, 10506–10513.
17 J. Xia, J. W. Bacon and R. Jasti, *Chem. Sci.*, 2012, **3**, 3018–3021.
18 Z. Xia, S. H. Pun, H. Chen and Q. Miao, *Angew. Chem., Int. Ed.*, 2021, **60**, 10311–10318.
19 M. Takeda, S. Hiroto, H. Yokoi, S. Lee, D. Kim and H. Shinokubo, *J. Am. Chem. Soc.*, 2018, **140**, 6336–6342.
20 Q. Huang, Y. Wu, Y. Zhou, H. Liu, J. Wang, S. Wang and P. Du, *Synthesis*, 2020, **52**, 2535–2540.
21 Q. Huang, G. Zhuang, H. Jia, M. Qian, S. Cui, S. Yang and P. Du, *Angew. Chem., Int. Ed.*, 2019, **58**, 6244–6249.
22 Y. Xu, B. Wang, R. Kaur, M. B. Minameyer, M. Bothe, T. Drewello, D. M. Guldi and M. von Delius, *Angew. Chem., Int. Ed.*, 2018, **57**, 11549–11553.
23 K. Li, Z. Xu, H. Deng, Z. Zhou, Y. Dang and Z. Sun, *Angew. Chem., Int. Ed.*, 2021, **60**, 7649–7653.
24 Y. Yang, S. Huangfu, S. Sato and M. Juríček, *Org. Lett.*, 2021, **23**, 7943–7948.
25 L. Zhan, C. Dai, G. Zhang, J. Zhu, S. Zhang, H. Wang, Y. Zeng, C.-H. Tung, L.-Z. Wu and H. Cong, *Angew. Chem., Int. Ed.*, 2022, **61**, e202113334.
26 X. Zhang, H. Shi, G. Zhuang, S. Wang, J. Wang, S. Yang, X. Shao and P. Du, *Angew. Chem., Int. Ed.*, 2021, **60**, 17368–17372.
27 S. Wang, X. Li, G. Zhuang, M. Chen, P. Huang, S. Yang and P. Du, *Chem. Commun.*, 2021, **57**, 9104–9107.
28 J. Almond-Thynne, D. C. Blakemore, D. C. Pryde and A. C. Spivey, *Chem. Sci.*, 2017, **8**, 40–62.
29 C. Amatore, G. Le Duc and A. Jutand, *Chem.–Eur. J.*, 2013, **19**, 10082–10093.
30 M. Gille, A. Viertel, S. Weidner and S. Hecht, *Synlett*, 2013, **24**, 259–263.
31 X. Zhang, H. Liu, G. Zhuang, S. Yang and P. Du, *Nat. Commun.*, 2022, **13**, 3543.
32 E. R. Darzi and R. Jasti, *Chem. Soc. Rev.*, 2015, **44**, 6401–6410.
33 T. Iwamoto, Y. Watanabe, T. Sadahiro, T. Haino and S. Yamago, *Angew. Chem., Int. Ed.*, 2011, **50**, 8342–8344.
34 T. Iwamoto, Y. Watanabe, H. Takaya, T. Haino, N. Yasuda and S. Yamago, *Chem.–Eur. J.*, 2013, **19**, 14061–14068.
35 N. Geue, R. E. P. Winpenny and P. E. Barran, *Chem. Soc. Rev.*, 2022, **51**, 8–27.
36 D. Felder, B. Heinrich, D. Guillon, J.-F. Nicoud and J.-F. Nierengarten, *Chem.–Eur. J.*, 2000, **6**, 3501–3507.
37 Y.-Y. Xu, H.-R. Tian, S.-H. Li, Z.-C. Chen, Y.-R. Yao, S.-S. Wang, X. Zhang, Z.-Z. Zhu, S.-L. Deng, Q. Zhang, S. Yang, S.-Y. Xie, R.-B. Huang and L.-S. Zheng, *Nat. Commun.*, 2019, **10**, 485.
38 **http://supramolecular.org**.
39 D. B. Hibbert and P. Thordarson, *Chem. Commun.*, 2016, **52**, 12792–12805.
40 P. Thordarson, *Chem. Soc. Rev.*, 2011, **40**, 1305–1323.
41 K. Ikemoto, K. Takahashi, T. Ozawa and H. Isobe, *Angew. Chem., Int. Ed.*, 2023, **62**, e202219059.
42 M. Freiberger, M. B. Minameyer, I. Solymosi, S. Frühwald, M. Krug, Y. Xu, A. Hirsch, T. Clark, D. M. Guldi, M. von Delius, K. Amsharov, A. Görling, M. E. Pérez-Ojeda and T. Drewello, *Chem.–Eur. J.*, 2023, **29**, e202203734.
43 S. Grimme, S. Ehrlich and L. Goerigk, *J. Comp. Chem.*, 2011, **32**, 1456–1465.
44 S. Miertuš, E. Scrocco and J. Tomasi, *Chem. Phys.*, 1981, **55**, 117–129.